Journal of Solid State Chemistry **142,** 74–79 (1999)
Article ID jssc.1998.7987, available online at http://www.idealibrary.com on IDEAL®

Defect Structure of Li-Doped BPO_4: A Nanostructured Ceramic Electrolyte for Li-Ion Batteries

M. J. G. Jak, E. M. Kelder, and J. Schoonman

Delft Interfaculty Research Center: Renewable Energy, Laboratory for Inorganic Chemistry, Delft University of Technology, Julianalaan 136, 2628 BL, Delft, The Netherlands

Received March 30, 1998; in revised form July 28, 1998; accepted August 2, 1998

In this paper the defect chemistry of Li-doped BPO_4 (BPO_4–xLi_2O, $0 \leq x \leq 0.1$) is studied. This nanostructured ceramic electrolyte is used in all-solid-state Li-ion batteries. By changing the Li-doping level the influence on the crystal structure is studied and related to the properties of the material. X-ray diffraction, Fourier-transformed infra-red spectroscopy (FT-IR), ^{31}P, ^{11}B, and ^{7}Li magic-angle-spinning solid state nuclear magnetic resonance, neutron diffraction, and inductively coupled plasma optical-emission spectroscopy measurements are used in order to study the structure. The electrical properties are studied with AC-impedance spectroscopy (AC-IS). The experimental data show that the defect structure of Li-doped BPO_4 can be described with two defect models, $Li_B'' + 2Li_i$ and $V_B''' + 3Li_i$, suggesting that the ionic conductivity takes place via interstitial Li ions. © 1999 Academic Press

Key Words: **defect chemistry; Li ion electrolyte; nanostructured ceramic; Li-doped BPO_4.**

INTRODUCTION

The structure of undoped BPO_4 has been studied in detail since the late 1930s and has been determined as the high-cristoballite structure (1–3). In this structure all the B and P ions are tetrahedrally coordinated by O ions and each O ion shared by two tetrahedra (Fig. 1). Kelder *et al.* (4) demonstrated the use of Li-doped BPO_4 as a Li ion conducting electrolyte for Li-ion batteries. A maximum in total ionic conductivity was found for a doping level of 7 mol.% Li. The maximum conductivity and conduction mechanism could be explained with a defect model for Li-doped BPO_4. However, a defect model for Li-doped BPO_4 has not been reported before. In order to derive a defect model, a number of techniques were used on Li-doped BPO_4 with doping levels of 0, 1, 2.5, 5, 7.5, 10, 15, and 20 mol.% Li. The BPO_4–xLi_2O powders were synthesized with two different synthesis methods; the phosphorus pentoxide (P_2O_5) synthesis route and the ammonium phosphate ($H_2NH_4PO_4$) synthesis route.

EXPERIMENTAL

Powders of BPO_4–xLi_2O ($0 \leq x \leq 0.10$, i.e., 0 to 20 mol.% Li) are synthesized either by the phosphorus pentoxide (P_2O_5) synthesis route (5) or the ammonium phosphate ($H_2NH_4PO_4$) synthesis route (4). Subsequently, the powders are ball-milled (Fritsch Pulverisette 7) down to an agglomerate size smaller than 10 μm. The overall Li, B, and P content of the samples is investigated with inductively coupled plasma–optical emission spectroscopy (ICP-OES) (Perkin Elmer Plasma II). During the exothermal synthesis an acid vapor is released. A small fraction of this vapor is captured in demineralized water and analyzed with ICP-OES in order to determine qualitatively the acid in this vapor. With X-ray diffraction (XRD) (Philips PW 1840 diffractometer with a Cu$K\alpha$ source) and neuron diffraction (ND) the structure of the samples is checked and the lattice parameters and primary particle sizes are calculated. The spectra are fitted by using PEAKFIT version 4 software (6). The P–O and B–O vibrational frequencies and their absorption as a function of the lithium doping level are determined with FT-IR measurements (Perkin Elmer Spectrum 1000). For these measurements pellets of 200 mg KBr with 0.5 mg BPO_4–xLi_2O powder are pressed.

The chemical environment of P, B, and Li is investigated with ^{31}P, ^{11}B, and ^{7}Li magic angle spinning–solid state nuclear magnetic resonance (MAS-NMR) (Varian VXR 400S with Doty Scientific Inc. probe). Reference materials for the ^{31}P, ^{11}B, and ^{7}Li MAS-NMR measurements are H_3PO_4 (1%), H_3BO_3 (0.1 M), and LiCl (0.1 M), respectively.

After analysis of the BPO_4–xLi_2O powders Magnetic Pulse Compaction (MPC) (5,7) is used to make pellets for the AC-IS measurements. A pressure pulse of approximately 1.28 GPa for 200 μs is applied. As a result pellets with a diameter of 15.0 mm and a thickness of approx. 1.5 mm are obtained. The density is about 80% of the theoretical X-ray density.

The ionic conductivity of MPC compacted samples with sputtered Pt electrodes (Edwards S150B sputter coater) is

0022-4596/99 $30.00

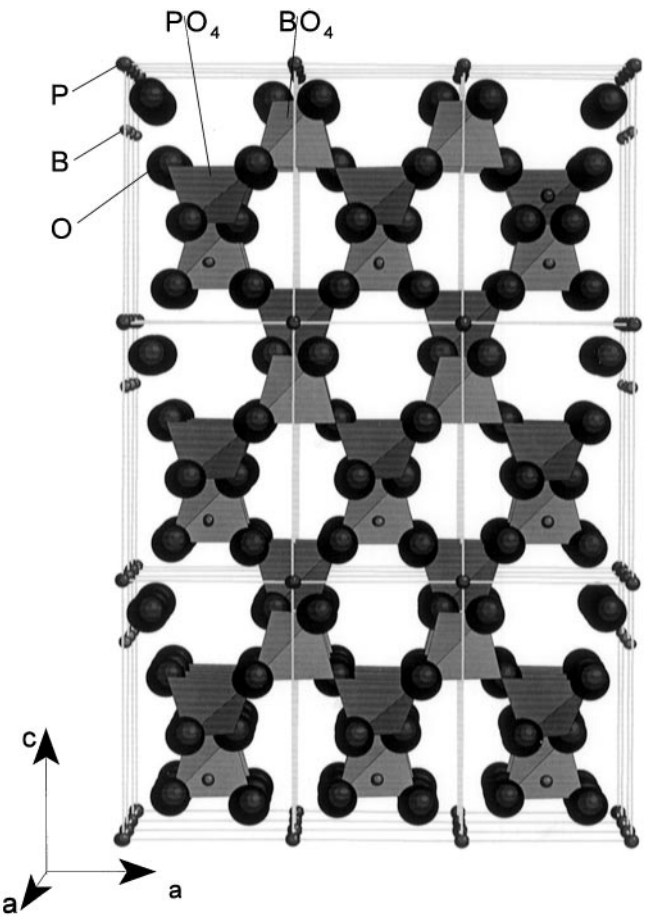

FIG. 1. Crystal structure of undoped BPO_4 (not to scale).

determined with AC-IS measurements (Schlumberger Solartron 1260). The measurements are performed in the frequency range from 0.1 Hz to 30 MHZ, while a voltage amplitude of 50 mV is applied. Measurements are performed in the temperature range of 40 to 600°C under air or N_2.

RESULTS

The *a*- and *c*-axes of the tetragonal high-cristoballite structure are calculated from fitted XRD spectra. For both syntheses a slight increase of the *c*-axis and a slight decrease of the *a*-axis is observed. The increase of the *c*-axis from 0 to 20 mol.% Li is about 0.2 and 0.3% for the P_2O_5 and $H_2NH_4PO_4$ synthesis, respectively, and the decrease of the *a*-axis is about 0.3 and 0.2% for the P_2O_5 and $H_2NH_4PO_4$ synthesis, respectively. The cell volume of the P_2O_5-synthesized material decreases with 0.4%, while the cell volume of the $H_2NH_4PO_4$-synthesized material decreases with only 0.1%.

In the XRD spectra of all samples no second phases are found. A change in peak width is observed as a function of the Li doping level. By using the PEAKFIT software the integral width, β, defined by the peak area divided by the intensity, is calculated. With the Scherrer equation,

$$d = \frac{k\lambda}{(\beta_m - \beta_a)\cos\Theta}, \qquad [1]$$

the primary particle size, d (in nm), is calculated. λ is the X-ray wave length (Cu$K\alpha$) in nm, k is the shape factor (about 0.9) in radials, β_m is the measured integral width in radials, β_a being the apparatus width in radials, and Θ is half the diffraction angle in radials. The apparatus width β_a is 0.0026 rad at $2\Theta = 25^o$ determined with a reference material. In Table 1 the particle sizes as function of the doping level are listed. The primary particle size is the size of the coherent diffracting domains. The calculated primary particle size of both synthesis methods is between 10 and 45 nm, with a maximum particle size of 42 nm at 10 and 15 mol.% for the $H_2NH_4PO_4$- and P_2O_5- synthesis route, respectively.

In Table 1 the total peak area (fitted area of the 10 strongest peaks) as function of the doping level is listed for both syntheses. The total peak area is mainly determined by the reflections of B and P. The clear decrease in total peak area with increasing doping level indicates removal of B and/or P from lattice sites and/or substitution by a lighter element which has fewer electrons and, therefore, has a lower scattering coefficient. The total peak area of the XRD spectra cannot be fitted with the proposed defect models since the X-ray density of the material as well as the defect concentration changes. The X-ray density changes due to the addition of Li and the change in cell volume.

Rietveld refined neutron diffraction spectra do not show any second phases either. The decrease in peak area is also observed in these spectra.

TABLE 1
Particle Size Derived from XRD and Relative Total XRD Peak Area

Li-doping level [mol.%]	Particle size (XRD) [nm]		Relative total peak area (XRD) [%]	
	$H_2NH_4PO_4$	P_2O_5	$H_2NH_4PO_4$	P_2O_5
0	12	26	100.0	100.0
1	11	25	98.8	100.1
2.5	13	19	104.2	98.4
5	16	19	100.4	99.0
7.5	24	18	98.8	99.1
10	42	19	95.5	97.5
15	26	42	94.5	95.8
20	33	40	94.0	92.2

The peak positions and peak intensities in the FT-IR spectra of BPO_4–xLi_2O both depend on the Li-doping level. Due to the coupling of the PO_4 and BO_4 tetrahedra it is not possible to distinguish between P–O and B–O vibrational frequencies (8). The 1095 and 935 cm^{-1} vibrational frequencies are attributed to the P–O and B–O bonds (9). The peak positions of the 935 and the 1095 cm^{-1} peaks shift to a lower value for both the P_2O_5 as well as the $H_2NH_4PO_4$ synthesis. This shift to a higher bond energy is concordant with the decreasing cell volume determined from XRD measurements. A higher bond energy of the B–O and P–O bonds will decrease the cell volume. The intensity of the peaks (per mg of BPO_4–xLi_2O) show a decreasing trend with increasing Li-doping level, indicating a decreasing number of P–O and/or B–O bonds.This decrease is more pronounced for the P_2O_5 synthesis. The decreasing peak area of the XRD spectra with increasing doping level supports the suggestion of removal of B and/or P from lattice sites and, hence, a decrease in the number of P–O and/or B–O bonds.

MAS-NMR measurements on P_2O_5- and $H_2NH_4PO_4$-synthesized BPO_4–xLi_2O show no change in the B environment. A change in the P environment is observed (Fig. 2). When comparing the ^7Li spectra, a change in peak width of the main peak is observed. Furthermore, the intensity of the spinning side bands increases at higher Li-doping levels (Fig. 3). The increasing side bands indicate a more anisotropical environment of the Li ions. A minimum in peak width of the main peak is found at 2.5–7.5 mol.% Li (Fig. 4). This minimal peak width indicates that the Li ion mobility is the highest (10) in the range of 2.5–7.5 mol.% Li.

ICP-OES measurements on the synthesized powders result in the overall composition B, P, and Li. From the ICP-OES results the Li/B ratio is calculated and plotted in Fig. 5. The P concentration is constant in the entire Li-doping range.

Analysis of the released vapor during the $H_2NH_4PO_4$ as well as the P_2O_5 synthesis reveals that the vapor contains boric acid and no traces of P are found. Hence a stoichiometrical composition is not possible.

AC-IS measurements on the cell Pt|BPO_4–xLi_2O|Pt in the temperature range from 40 to 600°C are performed under air and N_2. In Fig. 6 the Arrhenius plot of an MPC pellet of 10 mol.% Li (P_2O_5 synthesis) is shown. No difference between the conductivity measured under air or N_2 is visible. The conductivity activation energy for this sample is 0.83 eV under both air and N_2. Similar pO_2 independent

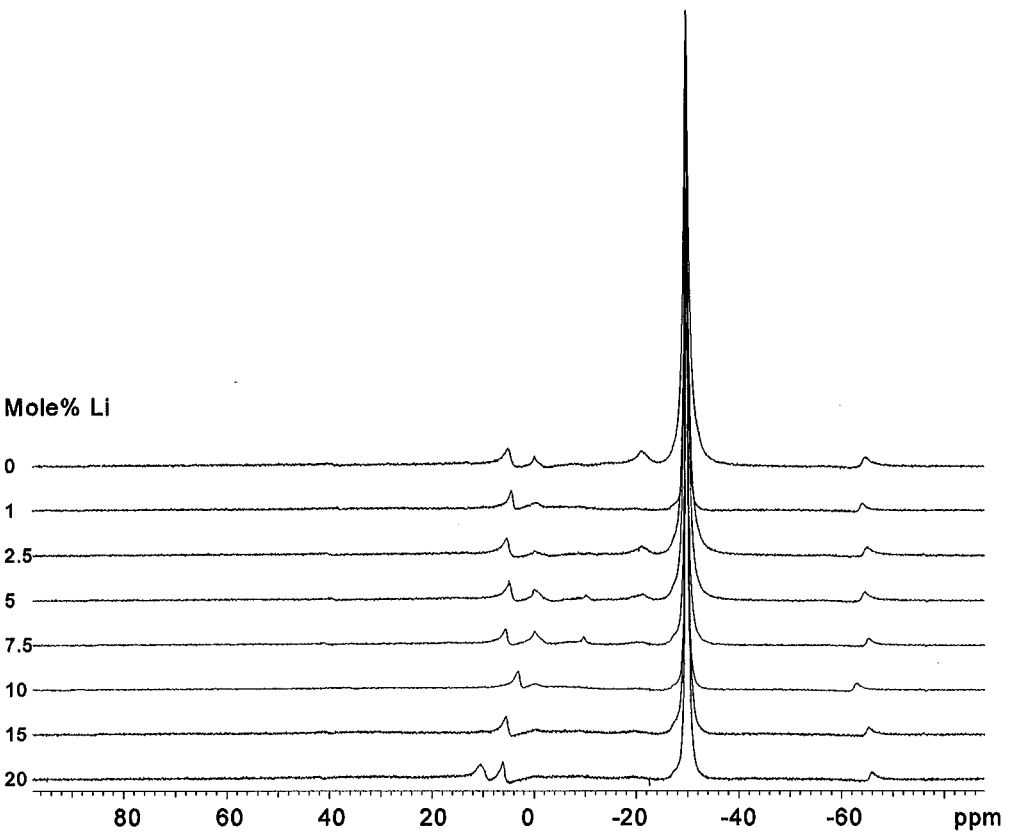

FIG. 2. ^{31}P MAS-NMR spectra of BPO_4–xLi_2O ($H_2NH_4PO_4$ synthesis).

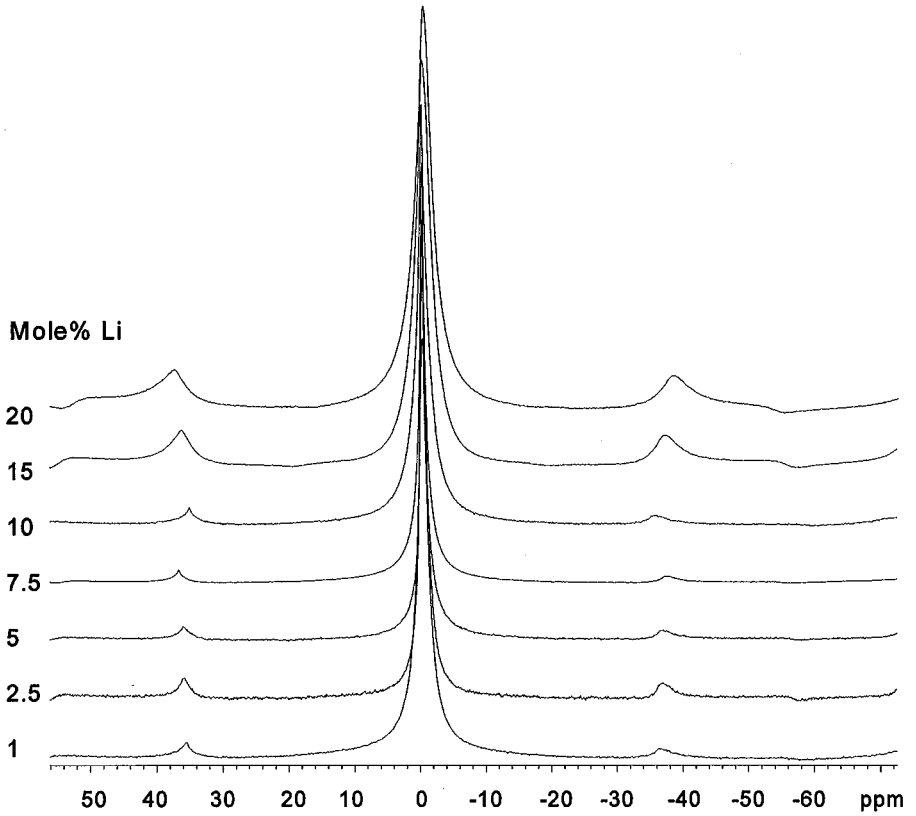

FIG. 3. ^{7}Li MAS-NMR spectra of BPO_4–xLi_2O ($H_2NH_4PO_4$ synthesis).

behavior is found for other samples. A detailed AC-IS analysis will be published in a forthcoming paper.

DISCUSSION

From a formal point of view, nine different defects can be assumed to be present in Li_xBPO_4:

$$\begin{gathered} Li''_B,\ Li'''_O \\ B''_P,\ P^{\cdot\cdot}_B \\ Li^{\cdot}_i,\ B^{\cdot\cdot\cdot}_i,\ O''_i \\ V^{\cdot\cdot}_O,\ V'''_B . \end{gathered} \qquad [2]$$

Defects with an effective charge of 4 and higher are energetically unlikely and, therefore, not taken into account.

In order to determine the validity of the remaining nine defects, the following summary of experimental results can be made:

(1) XRD and ND: a decrease in total peak area with increasing Li-doping level, indicating removal of B and/or P from lattice sites and/or substitutional replacement with a lighter element.

(2) FT-IR: decrease in the absorbtion of the 935 and 1095 cm^{-1} vibrational frequencies with increasing Li-doping level, indicating removal of P and/or B from PO_4 and/or BO_4 tetrahedrals, respectively. A change in the tetrahedral O coordination of B and/or P due to O loss should be observed by an additional peak of BO_3 and/or PO_3.

(3) ICP-OES: increasing loss of B during synthesis with increasing Li-doping level.

(4) MAS-NMR: change in mobility and environment of Li with different Li-doping level. Also different environments of P are found, but no changes in the B environment.

(5) AC-IS: No dependency of the ionic conductivity on the oxygen partial pressure.

All the oxygen related defects are excluded because of the independency of the conductivity on the oxygen partial pressure and by the FT-IR measurements, reducing the number of possible defects to six. The remaining possible defects will be discussed in detail below.

^{11}B MAS-NMR measurements show that only one B site ($B^{\times}_B$) is present. Therefore, the defects B''_P and $B^{\cdot\cdot\cdot}_i$ are in contradiction with this result since the presence of these two defects would result in different B environments which are not observed in the ^{11}B NMR spectra.

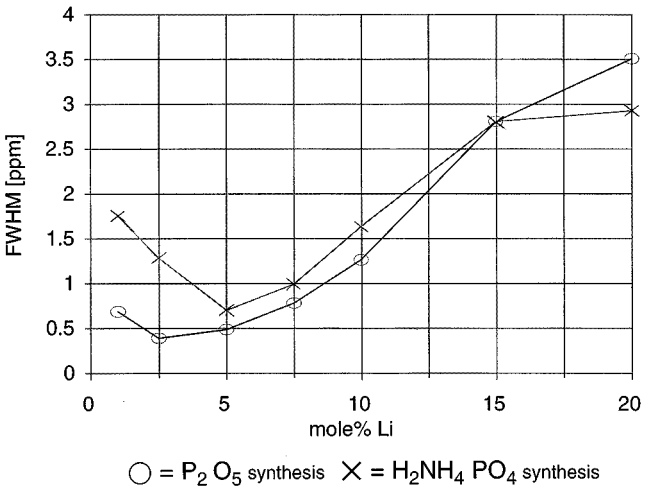

FIG. 4. FWHM of the ^{7}Li MAS-NMR main peak.

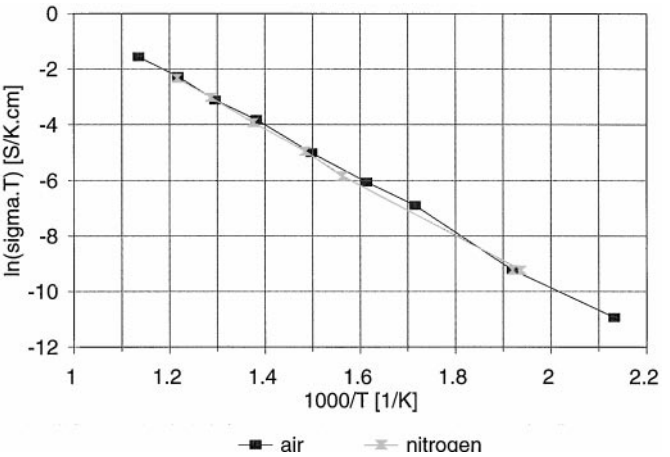

FIG. 6. Ionic conductivity of BPO_4–xLi_2O derived from AC-IS measurements performed under N_2 and air.

From the remaining four defects ($P_B^{\cdot\cdot}$, V_B''', $Li_i^{\cdot}$, Li_B'') combinations are made which obey the charge neutrality condition. Three combinations that involve Li are possible:

$$\begin{aligned} &V_B''' + 3Li_i^{\cdot} \\ &Li_B'' + 2Li_i^{\cdot} \\ &Li_B''' + P_B^{\cdot\cdot}. \end{aligned} \qquad [3]$$

The three combinations are fitted with the Li/B ratio from the ICP-OES analysis. From Fig. 5 it is clear that the two combinations involving interstitial Li show an excellent fit to the ICP-OES results. The identical curves of these combinations are due to the similar Li/B ratio.

The third combination ($Li_B'' + P_B^{\cdot\cdot}$) is not supported by the XRD, ND, or the ICP-OES results. In case of this combination an increase instead of a decrease of the total peak area in the XRD and ND with increasing Li-doping level should be observed. The contradiction with the ICP-OES measurements is clear from Fig. 5. Rejection of the third combination leads to two different models:

$$\begin{aligned} &\text{Model A: } V_B''' + 3Li_i^{\cdot} \\ &\text{Model B: } Li_B'' + 2Li_i^{\cdot} \end{aligned} \qquad [4]$$

Models A and B are concordant with all the experimental results. Furthermore, preliminary Rietveld refinement of

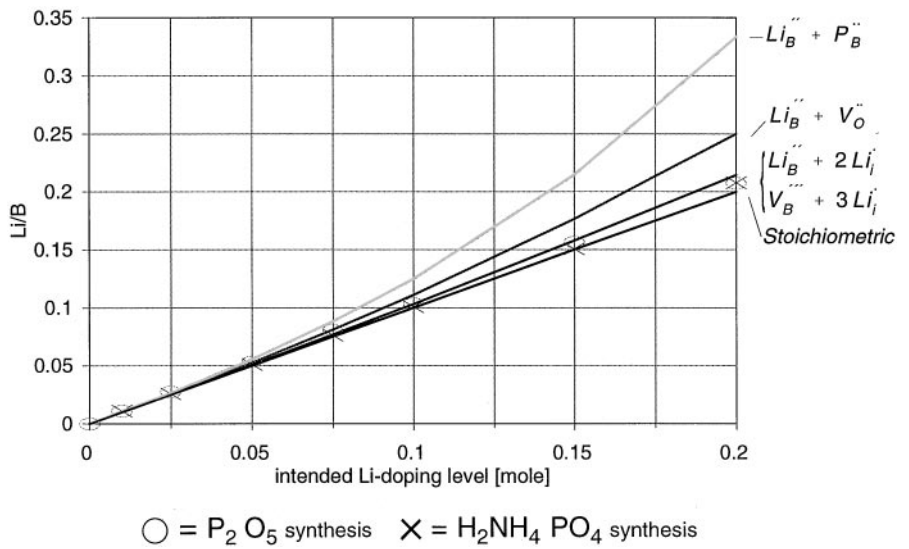

FIG. 5. Li/B ratio calculated from ICP-OES compared with the proposed defect models.

XRD data and ESCA (Electron Spectroscopy for Chemical Applications) measurements reveal two different interstitial Li sites. These interstitial sites can be seen between the tetrahedrals in Fig. 1.

Rewriting of models A and B leads to the following reaction equations:

$$x\mathrm{LiOH.H_2O} + \frac{x}{3}\mathrm{B_B^\times} \rightarrow \frac{x}{3}\mathrm{V_B'''} + x\mathrm{Li_i^\cdot} + \frac{x}{3}\mathrm{H_3BO_3}\uparrow + x\mathrm{H_2O}\uparrow \rightarrow (\mathrm{Li_i^\cdot})_x(\mathrm{B_B^\times})_{1-x/3}(\mathrm{V_B'''})_{x/3}(\mathrm{O_O^\times})_4 \quad \text{(Model A)}$$

$$x\mathrm{LiOH.H_2O} + \frac{x}{3}\mathrm{B_B^\times} \rightarrow \frac{x}{3}\mathrm{Li_B'''} + \frac{2x}{3}\mathrm{Li_i^\cdot} + \frac{x}{3}\mathrm{H_3BO_3}\uparrow + x\mathrm{H_2O}\uparrow \rightarrow (\mathrm{Li_i^\cdot})_{2x/3}(\mathrm{B_B^\times})_{1-x/3}(\mathrm{Li_B'''})_{x/3}(\mathrm{O_O^\times})_4 \quad \text{(Model B)} \qquad [5]$$

the overall reaction equation can be written as

$$x\mathrm{LiOH.H_2O} + \mathrm{BPO_4} \rightarrow \mathrm{Li}_x\mathrm{B}_{1-x/3}\mathrm{PO_4} + \frac{x}{3}\mathrm{H_3BO_3}\uparrow + x\mathrm{H_2O}\uparrow. \qquad [6]$$

CONCLUSIONS

Experimental data show that the defect structure of Li-doped BPO_4 can be described with the following defect models:

$$\text{Model A: } \mathrm{V_B'''} + 3\mathrm{Li_i^\cdot} \qquad \text{Model B: } \mathrm{Li_B''} + 2\mathrm{Li_i^\cdot} \qquad [4]$$

Based on Eq. [4] the Li-doped BPO_4 material can be described with the overall composition equation $\mathrm{Li}_x\mathrm{B}_{1-1/3x}\mathrm{PO_4}$.

The ionic conductivity takes place via interstitial Li ions. Ongoing NMR and Rietveld refinement of ND measurements will point out which defect model is valid or that both models coexist.

ACKNOWLEDGMENTS

The authors are grateful to Mr. F. de Lange and Mr. S. J. Everstein for their assistance with the powder synthesis and the XRD and FT-IR measurements. Mr. V. Verhoeven of the Interfacultary Reactor Institute of the Delft University of Technology is acknowledged for performing the ND experiments within the Delft Interfacultary Research Cluster (DIOC Sustainable Energy). Dr. Z. Kaszkur of the Institute of Physical Chemistry of the Polish Academy of Sciences provided the preliminary results on interstitial Li. Mr. A. Weisenburger (Institut für Neutronenphysik und Reaktortechnik, Forschungszentrum Karlsruhe, Germany) and Mr. W. J. Legerstee are thanked for their assistance with the MPC experiments. The European Science Foundation is acknowledged for traveling support to Germany and Poland via the ESF-NANO program. Finally, the Foundation for Chemical Research in The Netherlands (SON) and the Technology Foundation (STW) under the Netherlands Organization for Scientific Research (NWO) are gratefully acknowledged for financial support.

REFERENCES

1. G. E. R. Schulze, *Z. Physik. Chemie*, *B* **25,** 215 (1934). [in German]
2. K. Kosten and H. Arnold, *Z. Kristallogr.* **132,** 119 (1980). [in German]
3. B. P. Long, "Supplement to Mellor's Comprehensive Treatise on Inorganic and Theoretical Chemistry," 5 Section A13, pp. 651–654. Longman, London, 1975.
4. E. M. Kelder, M. J. G. Jak, F. de Lange, and J. Schoonman, *Solid State Ion.* **85,** 285 (1996).
5. M. J. G. Jak, E. M. Kelder, N. M van der Pers, A. Weisenburger, and J. Schoonman, *J. Electroceram.* **2,** 127 (1998).
6. PEAKFIT, version 4, Jandel Scientific Software, ALSN Software Inc., 1995.
7. M. J. G. Jak, E. M. Kelder, A. A. van Zomeren, and J. Schoonman, *in* "Exploratory Research and Development of Batteries for Electric and Hybrid Vehicles" (W. A. Adams, B. Scrosati, and A. R. Landgrebe, Eds.), PV96-14, p. 58. The Electrochemical Society Proceedings Series, Pennington, NJ, 1996.
8. C. E. Weir and R. A. Schroeder, *J. Res. Natl. Bur. Stand. A.* **68A,** 465–487 (1964).
9. F. Dachille and R. Roy, *Z. für Kristallogr.* **111,** 462 (1959).
10. M. A. París, A. M. Martínez-Juárez, J. M. Rojo, and J. Sanz, *J. Phys. Condens. Matter* **8**, 5355 (1996).